

# New Measurements with Stopped Particles at the LHC

Peter W. Graham<sup>1</sup>, Kiel Howe<sup>1</sup>, Surjeet Rajendran<sup>1,2</sup>, and Daniel Stolarski<sup>2,3</sup>

<sup>1</sup> *Stanford Institute for Theoretical Physics, Department of Physics, Stanford University,  
Stanford, CA 94305*

<sup>2</sup> *Department of Physics and Astronomy, Johns Hopkins University, Baltimore, MD 21218*

<sup>3</sup> *Center for Fundamental Physics, Department of Physics, University of Maryland,  
College Park, MD 20742*

## Abstract

Metastable particles are common in many models of new physics at the TeV scale. If charged or colored, a reasonable fraction of all such particles produced at the LHC will stop in the detectors and give observable out of time decays. We demonstrate that significant information may be learned from such decays about the properties (e.g. charge or spin) of this particle and of any other particles to which it decays, for example a dark matter candidate. We discuss strategies for measuring the type of decay (two- vs three-body), the types of particles produced, and the angular distribution of the produced particles using the LHC detectors. We demonstrate that with  $\mathcal{O}(10 - 100)$  observed decay events, not only can the properties of the new particles be measured but indeed even the Lorentz structure of the decay operator can be distinguished in the case of three-body decays. These measurements can not only reveal the correct model of new physics at the TeV scale, but also give information on physics giving rise to the decay at energy scales far above those the LHC can probe directly.

# Contents

<b>1</b>	<b>Introduction</b>	<b>1</b>
<b>2</b>	<b>Observing Decay Properties at the LHC</b>	<b>4</b>
2.1	Useful Measurements . . . . .	5
2.2	Detector Characteristics . . . . .	5
2.2.1	Measuring Jets . . . . .	6
2.2.2	Measuring Muons . . . . .	9
2.3	Stopping Particles . . . . .	10
<b>3</b>	<b>Distinguishing Decay Topologies</b>	<b>12</b>
<b>4</b>	<b>Determining Lorentz Structure</b>	<b>17</b>
4.1	Decay Operators . . . . .	17
4.2	Angular Distributions . . . . .	18
4.3	Testing MMCP Scenarios . . . . .	20
<b>5</b>	<b>Conclusions</b>	<b>21</b>

## 1 Introduction

The Large Hadron Collider (LHC) is currently probing physics at the weak scale. The discovery of new particles at the weak scale would tremendously enhance our understanding of TeV scale physics and could unveil the nature of the weak hierarchy problem. It is also possible that new particles could offer glimpses of physics at even higher scales. In particular, there may be metastable particles at the weak scale whose stability is violated by physics at very high scales. Generically, such particles will have lifetimes that are long on collider time scales ( $\gg$  ns). If these particles are colored or charged, they will be slowed down by electromagnetic interactions in the detectors at the LHC, causing a fraction of them to stop in these detectors [1, 2]. Observations of the eventual decay of these stopped particles can unmask their gauge quantum numbers, spin, and the nature of their physics responsible for its decay. In this paper, we present strategies to make measurements on the decays of stopped particles in the LHC detectors. Keeping in mind possible limitations of the detectors, we evaluate the prospects for identifying TeV and UV physics that couples these new particles to the Standard Model.

Massive metastable colored or electrically charged particles (MMCP, referred to in the draft as  $X$ ) generically arise if the particle is protected from rapid decay due to accidental symmetries of the low energy Lagrangian that are nevertheless violated by physics in the ultraviolet. The possible decay of the proton caused by the presence of GUT scale interactions that violate the

accidental baryon number symmetry of the standard model is a well known example of this phenomenon. It is possible that new particles at the TeV scale may exhibit similar features leading to metastability. There are a variety of such models in the literature [3, 4, 5, 6, 7, 8, 9, 10, 11, 12, 13, 14, 15, 16, 17, 18, 19].

Metastable particles that carry color (SIMPs) or electric charge (CHAMPs) emerge naturally in several scenarios of physics beyond the standard model (for general reviews see refs. [20, 21]). In supersymmetric (SUSY) models, particularly those where SUSY is broken below the intermediate scale of  $\sim 10^{11}$  GeV such as low scale gauge mediation, the gravitino naturally emerges as the lightest supersymmetric particle (LSP) of the SUSY spectrum. If SUSY breaking preserves  $R$ -parity, all the superpartners will ultimately have to decay to the gravitino. The gravitino has suppressed couplings to the rest of the superparticle sector. Consequently, the superpartners produced at the LHC will rapidly decay to the next to lightest supersymmetric particle (NLSP). But, the decays of the NLSP to the gravitino will be slow owing to the suppressed coupling of the NLSP to the gravitino, leading to a metastable NLSP [22, 23, 24]. Examples of charged NLSPs include stau ( $\tilde{\tau}$ ) and chargino ( $\chi^+$ ), while a colored one could be gluino ( $\tilde{g}$ ) or stop ( $\tilde{t}$ ), any of which would give rise to stopped particles at the LHC in this SUSY scenario.

Another SUSY scenario with metastable NLSPs emerges from SUSY theories which incorporate the axion mechanism [25] to solve the strong CP problem and have an axino LSP [26]. Like the gravitino, the axino's couplings are suppressed by a high scale making the NLSP long lived. Split supersymmetry [27] is a scenario in which the gluino is typically long lived and can often be stopped [2]. While metastability due to high scale physics is well motivated, the new particle may be long lived because of very small marginal couplings, such as in  $R$ -parity violating SUSY [28] or TeV scale See-Saw [29, 30, 31]. Within SUSY, there are methods to determine the reason that a particle is long lived [32]. Here we will mostly focus on longevity from low energy symmetries broken at high energy, but we will also briefly consider the case of very small  $R$ -parity violation.

If such a new particle is discovered at the LHC, it will be crucial to directly measure as many of its properties as possible in order to determine the underlying physics models. Heavy  $X$  particles are often produced with a velocity slower than the speed of light. This fact has been exploited to show how to make mass measurements by using time of flight information [24, 33, 34], and searches have been done at LEP [35, 36, 37], the Tevatron [38, 39, 40], and the LHC [41, 42, 43, 44] which place bounds on MMCP production. Other theoretical studies have shown that the LHC can exploit slow moving charged or colored particles to measure their spin [45, 46, 47, 48], color representation [48], flavor content [49, 50], polarization [51], masses of other new particles [52, 53, 54], as well as its coupling to the Higgs and other standard model particles [55, 56].

While much can be learned by studying the production and propagation of  $X$  particles at the LHC, there is interesting physics that can only be learned by studying their decays. For example, if the MMCP decays to an invisible particle, then studying the decay can measure some of the

properties of a potential dark matter candidate such as the mass. Measurement of the  $X$  lifetime can also give information about the particles that interact with both the MMCP and the dark matter candidate. Previous proposals to study decays of  $X$ s have included many creative ideas. One suggestion is to use the tracking systems to determine where an  $X$  exited the detector and is likely to have stopped, and then extract cores of the rock surrounding the detector likely to contain an  $X$  [57]. These  $X$  containing rock cores could then be studied in a quieter environment. A more ambitious possibility is to build a stopper detector just outside the main detector which can capture a fraction of the  $X$  particles and then measure their decay properties [58, 59, 60].

While these proposals could be implemented in the far future, it is interesting to see what measurements can be made with the detectors that are already in place. There is a substantial region of parameter space where many  $X$  particles will be stopped in the LHC detectors, especially once the LHC gets up to design energy and luminosity [2]. Furthermore, the LHC's detectors themselves generally stop far more MMCPs than a potential stopper detector would [59]. It is therefore interesting to ask what properties of  $X$  and its decay products can be measured by studying decays of particles stopped in the detectors. This is quite challenging, however, because the LHC detectors were designed to measure particles coming from a central interaction point, while in our case the event originates elsewhere. Despite these difficulties, both the D0 [61] and CMS [62, 63] have performed searches for decays of stopped particles, demonstrating that difficult experimental issues such as triggering can be solved.

In most models with stopped particles, the particle decays to visible standard model states (*i.e.* jets, charged leptons, photons *etc.*) and another heavy, neutral particle that leaves the site of the decay as missing energy. Unless otherwise noted, we will assume that the stopped particle decays with this topology. In some models, the invisible particle could be the dark matter particle, and we will refer to it as weakly interacting massive particle (WIMP), but the only fact we use is that it does not interact with the LHC detectors. This is generally a conservative assumption, as our proposals could be enhanced if the kinematic properties of the extra particle were directly observable.

We focus on measurements of the identity and kinematic distribution of standard model particles in the late decay of an  $X$ . A first observation is that the kinematics of the decay can often give information of the mass of the initial state as well as the invisible final state if the visible final state is understood. Previous studies have shown that it is in principle possible to measure the scale suppressing the operator which mediates decays as well as the spins of the  $X$  in the context of certain models without taking into account experimental realities [64, 65]. More realistic studies have demonstrated how to measure the lifetime [66, 67], and how to measure the origin of its longevity [32]. Here we demonstrate that the topologies and kinematic distributions of late decays can realistically be measured at the LHC, which can reveal the properties of TeV-sector particles as well as test and motivate models of UV physics responsible for the decay.

This paper is organized as follows. In Section 2, we examine the capabilities of the LHC detectors to measure the identity and kinematic distribution of the standard model particles produced in a late decay. We apply this in Section 3 to determine the ability of the LHC to distinguish MMCP scenarios based on the decay products in several motivated scenarios and in general. In Section 4 we focus on MMCPs with three-body decays and determine to what degree the LHC can distinguish models with particles of different spin and interactions of different Lorentz structure. We then conclude.

## 2 Observing Decay Properties at the LHC

The primary purpose of this paper is to provide theoretical guidance for the types of measurement and accuracy which would be necessary to distinguish different scenarios of late decaying particles at the LHC or beyond. Our measurement strategy begins with the identification of the number and type of visible standard model particles produced in the decay. Combining this information with kinematic measurements such as the angles between the final state particles, we can distinguish between a wide variety of physics scenarios.

In the case of two-body decays, the kinematics are trivial and contain no information. One can still identify the visible standard model particles in the decay and use this information to constrain the structure of the decay operator. But, there will nevertheless be degeneracies between different classes of UV operators that give to the same standard model decay topology. For three-body decays, there is additional information encoded in the kinematic distribution of the decays, and we present experimentally robust observables that can be used to extract this information. In some cases the UV model can lead to decays where both the two and the three-body decay modes have comparable branching fractions. It is therefore also important to be able to measure the branching fraction of these multiple decay modes since that can unveil the unique UV structure that allows these multiple modes to compete.

Obviously the capabilities of the ATLAS and CMS detectors to measure the properties of late decays must ultimately be determined by detailed detector simulations and studies. However, because these decays have unusual experimental signatures, it is useful to discuss in detail some of the experimental challenges that motivate our choices of observables. In Section 2.1, we summarize the type of measurements we believe are possible with late decays. In Section 2.2, we examine the physical features of the LHC detectors and estimate the ability of the detectors to measure properties of jets and leptons. We further discuss how these capabilities can be used to measure statistical kinematic properties of the decays. In Section 2.3, we study production and stopping of  $X$  particles and estimate the cross section and mass reaches of our measurement techniques.

## 2.1 Useful Measurements

Our conclusions in the following sections will rely on the ability to determine the properties of the primary SM decay products in a significant fraction of observed MMCP decays at ATLAS and CMS. As described in detail below, the most durable observables will be the multiplicity and direction of jets and hard muons in the final state of the decay chain. It is plausible that the direction of jets can be measured within an uncertainty of  $10^\circ - 30^\circ$ . Measurements of hard muon direction and multiplicity can be made with even higher accuracy, and it will be the accuracy for jets which is the limiting factor for our strategies.

In addition to particle identification, kinematic measurements will be useful if we are lucky enough to discover an MMCP which has a substantial branching fraction to a three-body (or higher) decay mode. In that case, the direction of final state jets and muons can be used to crudely reconstruct the decay. As discussed in Section 1, we will focus on three-body decays where one of the final states is invisible, while the other two are SM particles which interact with the detector (our methods still apply and likely could be improved if all of the particles produced are visible, e.g. in RPV decays). An example of the types of decays we are considering is shown in Figure 1. Of particular interest will be the distribution of the angle  $\theta_{12}$  between the two primary visible particles in the decay. Based on the uncertainty in jet angle measurement, we will take benchmarks of  $\Delta\theta_{12} \approx 10^\circ$ ,  $30^\circ$ , and  $60^\circ$  for the uncertainty in this measurement.

## 2.2 Detector Characteristics

The vast majority of stopped particles in ATLAS and CMS will come to rest in the central electronic and hadronic calorimeters [2]. Therefore searches for late decays at ATLAS and CMS [62] look for energy deposits in the hadronic calorimeter occurring out of time with beam crossings.

For the purposes of identifying decay products, this scenario has two advantages over the usual situation of a resonance or in-flight decay. First, because the MMCP decays at rest, the initial center of mass frame is known. Second, because the decays occur out-of-time from beam crossings, there is no event-by-event background from pile-up or the underlying event. Furthermore, there is no statistical background from e.g. hard QCD processes, which obviously do not occur out-of-time with beam crossings. The disadvantage is that because the decay occurs far away from the collision point, the ability to identify and measure the kinematic properties of particles is very diminished by the geometry of the calorimeters and the absence of information from the inner detector.

When interactions occur at the collision point, the fine segmentation of the calorimeters in the transverse  $\eta \times \phi$  plane allows good reconstruction for the direction of isolated energy deposits, even without tracking information. When the decay vertex is in the calorimeter, the geometry of the detector is no longer projective in the decay angles. Furthermore, the energy readout in

the calorimeters is sensitive to the location and orientation of an event relative to the active and inactive components of the calorimeter cells, and it is unlikely that the visible energy can be measured reliably on an event-by-event basis<sup>1</sup> for decay vertices inside the calorimeters.

A promising observable however is the geometric pattern of energy deposition in the calorimeter cells, which could reveal the direction of the primary particles and the location of the decay vertex. Electromagnetic energy will penetrate relatively few calorimeter cells, and it is therefore unlikely that useful directional information can be obtained from pure electromagnetic energy deposits except in the small fraction of decays producing products that pass back through the inner detector or into the muon chambers. Hadronic products will however deposit their energy over several nuclear interaction lengths, which corresponds to several cells in the HCAL and many cells in the ECAL. It therefore seems likely that directional information about jets can be obtained.

Another promising observable is hard muons, which will generally escape the calorimeters to pass through the muon chambers and are therefore straightforward to measure. However, cosmic muons are the dominant background for late decays so this must be considered carefully.

Motivated by these considerations, we will consider how jets and muons produced in late decays can be measured at the LHC detectors. We will then address how these measurements can be used to statistically distinguish between MMCP decay modes containing different primary particles, and further to measure the kinematic distributions of the primary particles.

### 2.2.1 Measuring Jets

The radial segmentation of the calorimeters is poor at both ATLAS and CMS.<sup>2</sup> It is therefore not straightforward to simply reconstruct a 3D track from the pattern of energy deposits. A possible search strategy is to restrict our attention to decay vertices located in the ECAL, for which it is simple to identify two points from which the trajectory can be constructed. Colored particles will produce jets with EM and hadronic components. The electromagnetic component will be primarily absorbed in the ECAL. The hadronic component can in general escape the ECAL (at ATLAS and CMS the ECAL has an annular radius of about one nuclear interaction length, while typical hadronic components deposit significant energy over a distance of about five interaction lengths [68]).

Depending on the angle of the final state visible particle relative to the detector geometry, different trajectories are possible. If the momentum is pointing radially outward, the radiation will leave the ECAL and directly enter the HCAL and further shower. If the momentum is pointing inward, it will leave the ECAL into the central tracker, deposit some tracks, then re-enter the calorimeters in a different region. A small fraction of the events will have a very small radial

---

<sup>1</sup>It seems likely, however, that for a large number of decays, the statistical distribution of energies could be used to roughly determine the MMCP-WIMP splitting from the average visible decay energies.

<sup>2</sup>At ATLAS the electromagnetic and hadronic calorimeters are each read out in two narrow and one thick central radial shells, while at CMS the ECAL has a single radial readout, and the HCAL has two.

	ATLAS	CMS
ECAL inner radius ( $R_{\text{ECAL}}$ )	115 cm	129 cm
ECAL instrumented annular radius ( $\Delta R_{\text{ECAL}}$ )	47 cm	23 cm
HCAL inner radius ( $R_{\text{HCAL}}$ )	228 cm	175 cm
HCAL instrumented annular radius	164 cm	96 cm
ECAL $\eta \times \phi$ resolution	$0.025 \times 0.025$	$0.0174 \times 0.0174$
HCAL $\eta \times \phi$ resolution	$0.1 \times 0.1$	$0.087 \times 0.087$

Table 1: Geometric properties of the barrel components of the CMS and ATLAS calorimeters from [70, 71, 72, 73, 74, 75].

momentum and stay confined to the ECAL, but here we focus on the majority of events where some radiation escapes the ECAL. The geometry is shown in Figure 1 for a decay originating in the ECAL with two jets in the final state. We note that this figure is schematic and the angular resolution of the calorimeters is much finer than the depiction in the figure. The relevant geometric properties of the ATLAS and CMS detectors are summarized in Table 1. Also relevant is the nuclear interaction length  $\lambda_I \sim 20$  cm for the absorbing components of the calorimeters.

Due to the poor radial segmentation of the ATLAS and CMS calorimeters, the uncertainty in the measurement of  $\theta_{12}$  is dominated by the radial uncertainty not the resolution in  $\eta \times \phi$  plane. For particles that exit the ECAL into the central tracker, like the jet going down the page in Figure 1, it is simple to estimate the angular resolution achievable. The first point in the trajectory is the decay vertex, which can be located in the  $\eta \times \phi$  plane through the shape of the deposit of EM energy in the ECAL. The radial uncertainty is given by the annular radius of the ECAL,  $\Delta R_{\text{ECAL}}$ . The second point on the trajectory is the location where the energy deposit re-enters the ECAL. The characteristic angular resolution for this method is simply estimated in terms of the ECAL inner and annular radii,

$$\Delta\theta \sim \frac{\Delta R_{\text{ECAL}}}{R_{\text{ECAL}}}. \quad (1)$$

For ATLAS,  $\Delta\theta \sim 25^\circ$ , and for CMS it is even better,  $\Delta\theta \sim 10^\circ$ .

For particles like the jet going up the page in Figure 1 which go directly from the ECAL to the HCAL, the second point in the trajectory is the center of the HCAL energy deposit, which will occur in one of the nearby cells. The uncertainty in angle can be estimated from the distance  $R_{E-H}$  between the radial centers of the ECAL and HCAL cells to be  $\Delta\theta \approx \frac{\Delta R_{\text{ECAL}}}{R_{E-H}}$ , with



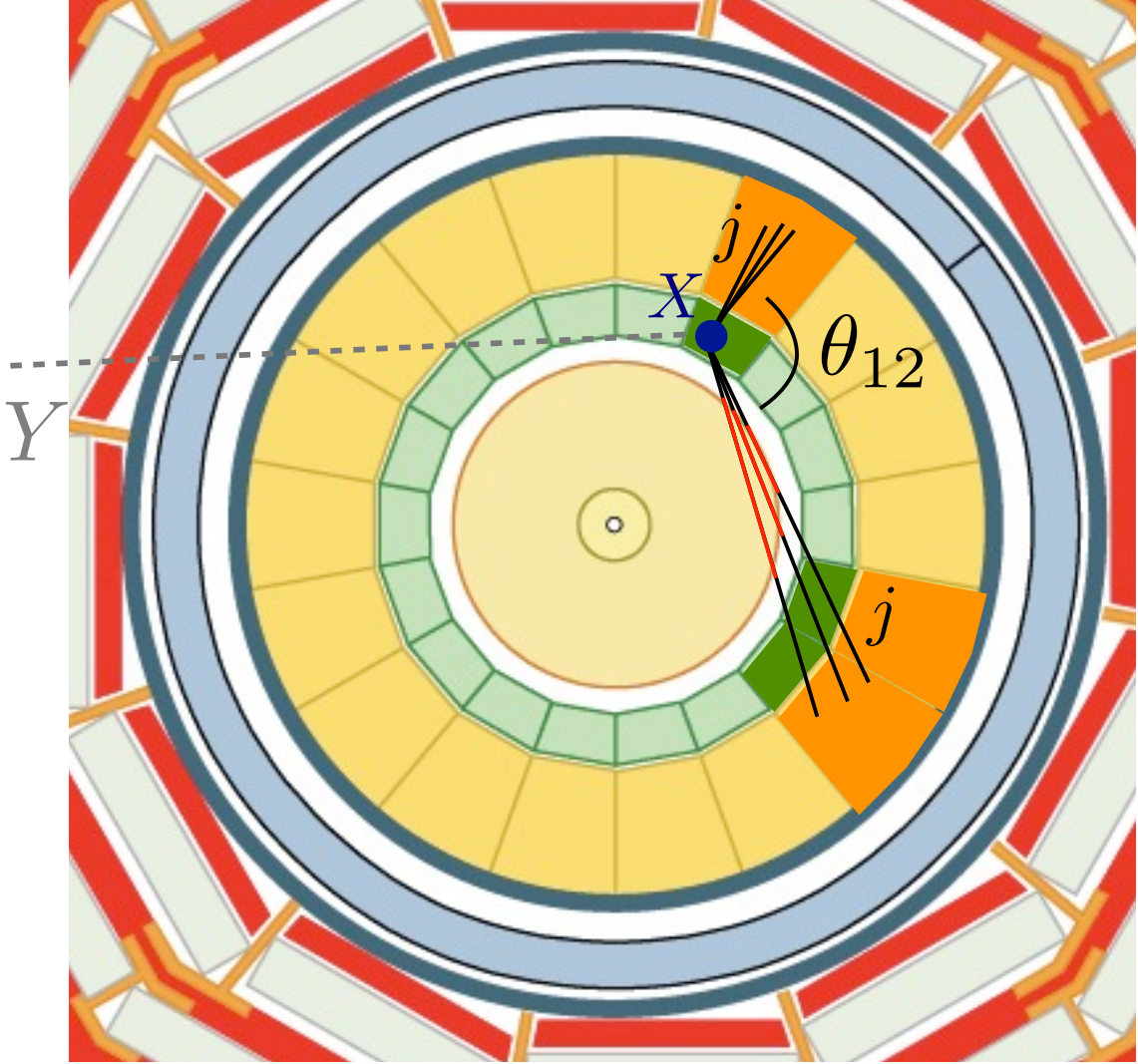


Figure 1: A schematic view of the event geometry we are considering. This is a cross sectional  $x-y$  view of a detector taken from [69]. The inner circle is the tracking chamber, the next (green) section is the electromagnetic calorimeter, followed by the (orange) hadronic calorimeter. The outermost layers are the muon chambers. An MMCP  $X$  that had stopped in the ECAL decays into two jets and an invisible  $Y$  which escapes the detector without interacting. The ECAL cell where the decay took place shows energy deposition. One of the jets exits the ECAL and deposits its energy into the HCAL. The second jet exits the ECAL in another direction, leaving tracks which do not point back to the interaction region, and then depositing energy in a different region of both the ECAL and HCAL. This is a schematic representation; the  $\phi$  resolution of the actual detector is much finer in both the ECAL and HCAL, so that the cells that lit up in the calorimeter should give enough information to approximately determine  $\theta_{12}$ , the angle between the jets.

$\Delta\theta \sim 35^\circ$  for ATLAS and  $\Delta\theta \sim 25^\circ$  for CMS.

These simplified cases and geometric estimates suggest that a resolution of  $\Delta\theta \approx 30^\circ$  is plausible to expect for the measured angle between two jets, and that the geometry of CMS makes a slightly better measurement possible. Naturally the actual experimental precision will have a complicated and non-uniform dependence on angle due to the geometry and response of the detector; our purpose here is simply to roughly determine the accuracy attainable in a measurement after accounting for these effects. We have therefore also considered benchmarks of  $\Delta\theta \approx 10^\circ$  and  $\Delta\theta \approx 60^\circ$ .

Another source of uncertainty is the fact that colored particles undergo parton showers and hadronization and deposit energy in the form of jets. From jet shape studies [76], on average  $\sim 90\%$  of jet energy will be deposited within an angular cone of opening angle  $\theta_{\text{jet}} \sim 30^\circ$  at  $E = 100$  GeV. For a 1 TeV  $X$  particle, the jet energies will be somewhat higher making their opening angles moderately smaller, but this sets the rough limit on the relative angle at which two jets can be distinguished from one another, and is incidentally roughly the same as the overall angular resolution.

A more accurate method of making angular measurements might be possible through further study of the shapes of energy distributions in the calorimeter cells, as well as the possible incorporation of inner detector measurements of charged particles. However, our assumed resolution and accuracy is sufficient to demonstrate the plausibility of distinguishing many of the scenarios enumerated once  $O(100)$  events have been observed in the ECAL. Other possible strategies considered had roughly the same or worse accuracy and efficiency.

Finally, we comment on the more remote possibility of obtaining more detailed radial information from the calorimeters. For instance, the HCAL at CMS has 17 radial segments which are an average of about 6 cm thick. The current setup of CMS integrates this into two different readouts, so only very coarse transverse information is kept. If a long lived charged particle is discovered, however, the experiment may achieve significant gains in reconstruction of the decay points and jet direction within the HCAL by separately reading out each of the layers. This could allow for much better measurements of angular distributions and ultimately UV properties of the new stable particle.

### 2.2.2 Measuring Muons

Isolated muons can be produced as primary particles in an  $X$  decay. Hard isolated and non-isolated muons can also be produced in secondary decays. For a decay originating in the ECAL, the muon direction can be measured from the location in  $\eta \times \phi$  of its entry into the barrel muon system, or in  $R \times \phi$  plane for the endcap muon systems.

One complication is that decays originating from the ECAL are less shielded, meaning that shower particles could possibly leak into the muon system. However, the material before the

HCAL only accounts for  $\sim 1\lambda_I$  of shielding, so the remaining shielding is likely adequate.

Another more serious complication is that in late decay searches, a muon veto is usually applied to reduce the cosmic background. If we wish to measure muons in late decay events, the cosmic background needs to be reduced in another way. The rate of cosmic muons expected to register  $E > 20$  GeV in the ATLAS HCAL is  $2 \text{ Hz} \approx 5 \times 10^6/\text{month}$  [77]. Because the cosmic spectrum falls off with energy, increasing the selection to  $E \gtrsim 500$  GeV would reduce the background by 3 orders of magnitude based on the measured spectrum [78], but the rate could still be comparable to the expected signal for higher mass  $X$  particles.

Muon momentum measurements could be used to veto cosmic muons with enough energy to cause such high energy events in the calorimeters. For example, the cosmic muon background vanishes below the horizon, so it may be possible to use track direction and timing measurements to veto the cosmic backgrounds while retaining a large fraction of signal events. One could also look for muons associated with jet activity in certain types of decays to discriminate signal from cosmic background. Another possible experimental observable when the MMCP lifetime is relatively short  $\lesssim 1$  s, is to look for temporal correlations in the cosmic muon spectrum. Because the MMCP must be pair produced, events where both stop in the detector and both have muons in the decay will give rise to a signal in these temporal correlations and could allow a measurement of the lifetime. It seems plausible that the background can be reduced in these ways, but a more detailed analysis is beyond the scope of this paper.

## 2.3 Stopping Particles

To interpret our results it will be useful to make an estimate of the necessary production cross sections and mass reaches. The  $X$  particles are slowed down in the detectors due to electromagnetic interactions between  $X$  and the electrons in the detector. For a heavy particle, the energy loss induced by these electromagnetic interactions imply that particles slower than a critical velocity are stopped in the detector and the fraction of stopped particles can then be computed from the velocity distribution of the produced  $X$ .

This velocity distribution depends upon both the production mechanism of  $X$  and the rest of the spectrum. If  $X$  is produced in the primary hard process, it will often be produced near threshold (due to PDF suppression) and will be slow. This is likely in the case of heavy colored  $X$ s such as the gluino. For direct pair production, scalars such as the stau and stop will tend to be produced with a harder spectrum than fermions like gluinos and charginos.  $X$  could also be produced as a result of cascade decays of heavier particles, in which case those particles will be more relativistic. This should be expected in the case of the long lived stau or chargino in supersymmetry, where it will be produced dominantly as a result of cascade decays from heavier colored particles. When  $X$  carries color, there is an additional source of uncertainty coming from the spectrum of charged R-hadron states and their propagation through the detector [2, 79, 80, 81].

There is thus some model dependence in estimating the number of stopped particles for a given  $X$ . We will give mass reaches with the conservative assumption that MMCPs are produced only by direct pair production. For example, at the LHC with  $\sqrt{s} = 14$  TeV, pair production of a color octet Majorana fermion (gluino) is one of the most favorable cases, with a cross section of 300 fb at 1 TeV, dropping rapidly to 10 fb for at 1.5 TeV [82]. On the other hand, a color neutral electrically charged scalar (right handed stau) is one of the most difficult cases with a Drell–Yan cross section of 100 fb at a mass of 100 GeV dropping to 10 fb at 200 GeV [83]. If there are other particles in the spectrum, they could dramatically increase the cross section, and this is the case in many scenarios.

To convert between event rates and cross sections we have calculated the direct production velocity distributions and compared to the critical stopping velocity. From ref. [2], a CHAMP of mass  $M$  and velocity  $\beta$  will travel a distance

$$x = x_0 \left( \frac{M}{500 \text{ GeV}} \right) \int_{\beta_0}^{\beta} \frac{\beta'^3 d\beta'}{1 + \log(\beta')/\kappa}. \quad (2)$$

For propagation in lead,  $x_0 = 503$  m,  $\kappa = 3.6$ , and  $\beta_0 \approx 0.05$ . The ATLAS and CMS ECALs have roughly the stopping power of 20 cm of lead, and the critical velocity can be found by solving for  $\beta$  given  $x = 20$  cm. For SIMPs, an  $\mathcal{O}(1)$  fraction will hadronize to charged R-hadron states and stop in the same way.<sup>3</sup> The additional hadronic interactions of SIMPs with the detector are unimportant here as on average  $\lesssim 1$  such interaction will take place before the particle leaves the ECAL [81]. Under these assumptions we find that the ECAL stopping fraction is  $\sim 0.25\%$  for the MMCPs considered in this work, with the exception of staus, for which only  $\sim 0.05\%$  stop in the ECAL for masses near  $M = 100$  GeV. This latter case has a significantly smaller stopping fraction because the scalar production spectrum is hard and unlike e.g. squark production, there is no enhancement from the low  $x$  gluon PDFs.

Discovery searches for MMCP late decays typically search for decays in the HCAL where roughly 4-10 times more MMCPs will stop than in the ECAL. Thus a measurement of particle properties from late decays in the ECAL will require 4-10 times more integrated luminosity than a discovery. To determine the 14 TeV LHC reach more quantitatively, we take as a benchmark a hypothetical dataset of  $200 \text{ fb}^{-1}$ . If a late decaying particle with lifetime  $\gtrsim 100$  ns is discovered, the proton bunch structure could in principle be optimized to allow the decays of  $\sim 50\%$  of produced MMCPs to be observed sufficiently out of time with any LHC collisions. Taking a further 50% trigger/cut efficiency for late decay searches [62], in such a dataset the number of late decays observed in the ECAL for a particle with pair production cross section  $\sigma$  will be

$$N = 25 \times \left( \frac{\sigma}{100 \text{ fb}} \right) \left( \frac{\delta}{0.25\%} \right). \quad (3)$$

---

<sup>3</sup>It is possible that the charged R-hadrons decay strongly to a neutral state, depleting the population of charged states before they reach the ECAL. However, such large splittings in the R-hadron mass spectra are disfavored [85, 86].

	N	$M$	$\sigma(M)$	$\delta(M)$
Q=0 color octet fermion (gluino)	10	$\sim 1300$ GeV	40 fb	0.25%
	100	$\sim 1000$ GeV	400 fb	0.25%
Q=2/3 color triplet scalar (stop)	10	$\sim 600$ GeV	50 fb	0.2%
	100	$\sim 400$ GeV	400 fb	0.25%
Q=1 SU(2) doublet fermion (higgsino)	10	$\sim 500$ GeV	33 fb	0.3%
	100	$\sim 300$ GeV	290 fb	0.35%

Table 2: The masses at which  $N = 10$  and  $N = 100$  observable late decay events are produced in the ATLAS or CMS ECAL with  $200 \text{ fb}^{-1}$  at the 14 TeV LHC, assuming only direct production as in Eq. (3). The relevant direct production cross section  $\sigma(M)$  and stopping fraction  $\delta(M)$  calculated at each mass are shown. For colored particles, only colored production was included. Tree level cross sections and velocity distributions calculated with MadGraph 5 [87], NLO cross sections for gluino from [82].

The MMCP mass and direct production cross section corresponding to event counts of  $N = 10$  and  $N = 100$  are shown for a few representative MMCP candidates in Table 2, based on stopping fractions calculated as described above. To get a feel for the numbers, consider a 1 TeV gluino. At the 14 TeV LHC with our benchmark set of  $200 \text{ fb}^{-1}$ , 120,000 gluinos will be produced yielding about 75 observed decays in the ECAL. As we will see in Sections 3 and 4, this is enough to distinguish Split SUSY from the majority of other possible scenarios. Most other MMCP candidates also have large enough direct production rates at the LHC for our methods to be applicable. However, for direct production of a right handed stau more than  $\sim 10$  decays in the ECAL will only be observed for a mass lighter than 90 GeV. This is excluded by LEP searches for long lived charged particles [84], and therefore our methods are only applicable to a stau MMCP when the total LHC production cross section is enhanced by cascades to the NLSP.

### 3 Distinguishing Decay Topologies

The MMCP decays we are considering usually produce one on-shell WIMP sector particle and a number of on-shell primary SM particles. The properties of these particles can distinguish different MMCP scenarios. However, extracting this information is complicated by the decays of heavy primary SM particles ( $W$ ,  $Z$ ,  $h$ ,  $t$ ) and the possible decay chain of the WIMP sector particle to the WIMP. In this section we discuss how these difficulties can be overcome and how the late decay observables described in Section 2 can be used to distinguish models with sufficiently different decay modes, e.g a Split SUSY gluino and a stau NLSP.

As discussed in Section 2 a measurable event is identified by a large localized energy deposit in the ECAL, and the observables for each such event are the jets and hard muons produced in addition to the electromagnetic energy deposit. We can therefore classify the topology of each observed event by  $n_j$ , the number of jets observed and  $n_\mu$ , the number of isolated hard muons observed. We will require  $n_j \geq 1$  to suppress calorimeter noise and cosmic ray backgrounds.

The branching fractions to SM decay modes can be translated into branching fractions for the different observable decay topologies. For an MMCP mass of order 1 TeV and a large splitting between the MMCP and invisible particle's mass, jets from primary ( $u, d, s, c, b$ ) quarks will be collimated and reflect the kinematic properties of the primary particle.<sup>4</sup> Heavy particles ( $W, Z, h, t$ ) will be produced with small boosts ( $\gamma \sim 2 - 5$ ), and although some directional information will be preserved, their decay products will lead to separated jets and muons.

If the MMCP decays directly to the stable WIMP, for instance in SUSY models where the NLSP decays to a gravitino or axino, then the WIMP will not produce an observable signal in the calorimeters. However, it is also possible that the WIMP forms part of a more complicated electroweakly interacting sector, e.g. the charginos and neutralinos in SUSY. Cascade decays to the WIMP state will then typically produce  $Z$ 's,  $W$ 's, and lighter SM particles. If the splittings are comparable to the WIMP mass, this can produce additional hard jets and muons in the event. Although such a cascade allows information to be determined about the WIMP sector particles, it also complicates the identification of the primary decay products. Fortunately, the cascade particles are typically softer than the primary decay particles and lead to higher multiplicity events, which can be exploited to explore the two sectors separately. We also consider a simple R-parity violating (RPV) scenario with a single dominant  $LLE^c$  RPV coupling to explore similar signals in the absence of an invisible WIMP and to explore a lepton rich final state (see Figure 3).

In Table 3, the branching fractions to different decay topologies are shown for several motivated MMCP scenarios (see caption) with parameters chosen to give similar LHC event rates and signatures. Because the overall event rate is a priori unknown, we consider only the branching ratios between observable states ( $n_j \geq 1$ ). The effect of different energy cuts and angular resolutions are shown for the gluino three-body decay and are representative of the effects on the other decay modes. The variation of the branching fractions with the energy cut-off and the angular resolutions suggests that the systematic uncertainties in branching fraction measurements will be  $\mathcal{O}(1\%)$  for muon modes and low-multiplicity jet modes, and  $\mathcal{O}(10\%)$  for high-multiplicity jet modes (there is a greater probability of jets overlapping for higher multiplicity modes, leading to greater uncertainty in identifying branching fractions). For the rest of the analysis we focus on the case  $\Delta\theta = 30^\circ$ .

The first observation is that decay modes with different numbers of primary colored particles

---

<sup>4</sup>Muons from bottom and charm decays could be associated with jets to identify the flavor structure of the decay, but here we will simply treat these muons as part of the jet.

Mode	$E_j(\text{GeV})$	$\Delta\theta$	1j	2j	3j	$\geq 4j$	$1\mu$	$2\mu$
A: $\tilde{g} \rightarrow qq'\chi_i^{0,\pm}$	50	$10^\circ$	1%	28%	26%	45%	13%	2%
	50	$30^\circ$	2%	30%	31%	37%	12%	2%
	50	$60^\circ$	5%	43%	41%	11%	9%	1%
	20	$30^\circ$	1%	21%	18%	60%	12%	1%
B: $\tilde{g} \rightarrow g\chi_i^0$	50	$30^\circ$	35%	31%	32%	2%	3%	3%
C: $\tilde{t}_1 \rightarrow \tilde{G}t$	50	$30^\circ$	35%	40%	25%	0%	8%	0%
D: $\tilde{\tau}_1 \rightarrow \tilde{G}\tau$	50	$30^\circ$	100%	0%	0%	0%	0%	0%
E: $\chi^+ \rightarrow \tau^-\tau^+\mu^+/\tau^+\nu_\tau\nu_\mu/\mu^+\nu_\tau\bar{\nu}_\tau$	50	$30^\circ$	90%	10%	0%	0%	42%	8%

Table 3: The branching fractions to final state topologies for several MMCP scenarios. Isolated final state (before parton showering) colored particles are identified as jets, and a cut of  $E > 20$  GeV was placed for muons and  $E > E_j$  as shown for jets. Jets from partons separated by  $\Delta\theta$  were considered distinct, and likewise muons were considered to be isolated when separated by greater than  $\Delta\theta$  from a colored parton. **Model A:** Split SUSY three-body gluino decay  $\tilde{g} \rightarrow qq'\chi_i^{0,\pm}$  summed over branching to all neutralinos, charginos, and SM states (see Figure 2) for a Bino-like LSP with low-energy mass parameters  $\mu = 200$  GeV,  $M_1 = 130$  GeV,  $M_2 = 260$  GeV, and  $m_{\tilde{g}} = 1$  TeV. **Model B:** Split SUSY two-body gluino decay  $\tilde{g} \rightarrow g\chi_i^0$ , same low energy parameters as for three-body decay. **Model C:** Stop NLSP two-body decay to gravitino / axino LSP for  $m_{\tilde{t}} = 600$  GeV and  $m_{\tilde{G}} = 10$  GeV. **Model D:** Stau NLSP two-body decay to gravitino / axino LSP for  $m_{\tilde{\tau}} = 150$  GeV and  $m_{\tilde{G}} = 10$  GeV. For (C) and (D) the small  $\mathcal{O}(1\%)$  branching fractions to primary three-body decays [88] are ignored. **Model E:** R-parity violating (RPV) decay of a  $\sim 400$  GeV higgsino-like chargino LSP through the superpotential operator  $L_3L_2E_3^c$  (see Figure 3) in the MSSM with weak-scale parameters  $M_1 = -800$  GeV,  $M_2 = 1600$  GeV,  $\mu = 400$  GeV and a GMSB-like scalar sector with masses  $\sim 3$  TeV. Numerical calculations performed using MadGraph 5 [87], BRIDGE [89], and SUSYHIT [90].

can easily be distinguished. For a given decay, the number of colored particles sets the minimum number of jets that will be present, regardless of the details of decays of secondary particles and WIMP sector cascades. For example, in Split SUSY, a long-lived gluino can dominantly decay either to a three-body mode or two-body mode through a loop as shown in Figure 2. Depending on the region of parameter space, either of the modes can dominate [91], and these two modes correspond to (A) and (B) in Table 3. In model (A), the branching fraction to  $1j$  is only 2%, with the small fraction coming from the second primary jet being too soft or collinear with the first jet. In (B) on the other hand, there is only one primary colored particle, and so the branching fraction to  $1j$  is 36%. Therefore only  $\mathcal{O}(10)$  observed decays are necessary to statistically distinguish (A) and (B) at the 95% confidence level. Model (A) can be distinguished from model (C) in the same way, and this method is fairly insensitive to the exact energy cuts and angular resolutions  $\Delta\theta$  used.

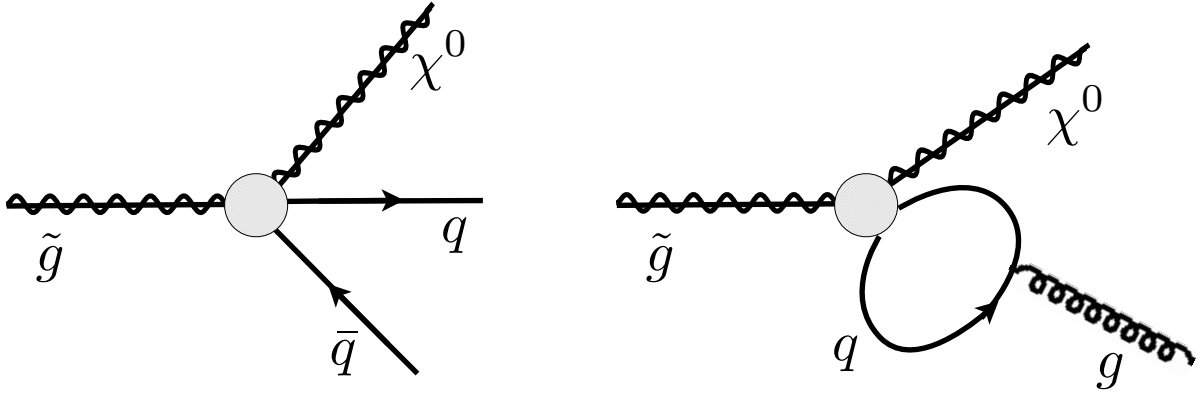


Figure 2: Feynman diagrams for the decays of a long lived gluino in Split SUSY. The blob represents the four point vertex generated after integrating out the heavy squark. The diagram on the left is a tree level three-body decay to two quarks and a neutralino, while the diagram on the right is the loop level two-body decay to a neutralino and a gluon. In certain regions of parameter space, the loop induced decay can become dominant over the three-body decay [91].

There is also a region of the Split SUSY parameter space where the two and three-body decays (A) and (B) have comparable branching fractions. In this case, a measurement can be made to determine the three-body branching fraction  $\Gamma_A$ , which can be used to determine the UV scale of the theory [92]. With  $\mathcal{O}(100)$  events observed,  $\Gamma_A$  can be determined to an accuracy of about  $\pm 10\%$ . This possibility is not restricted to Split SUSY; two and three-body decays can naturally compete in any model where three-body decays are mediated at a high scale and induce two-body decay at loop levels, and a similar measurement will be possible in such scenarios.

The only observable decay for model (D) involves the hadronic tau decay to a single jet, thus (D) can be ruled out by the observation of a significant fraction of higher jet multiplicity events.



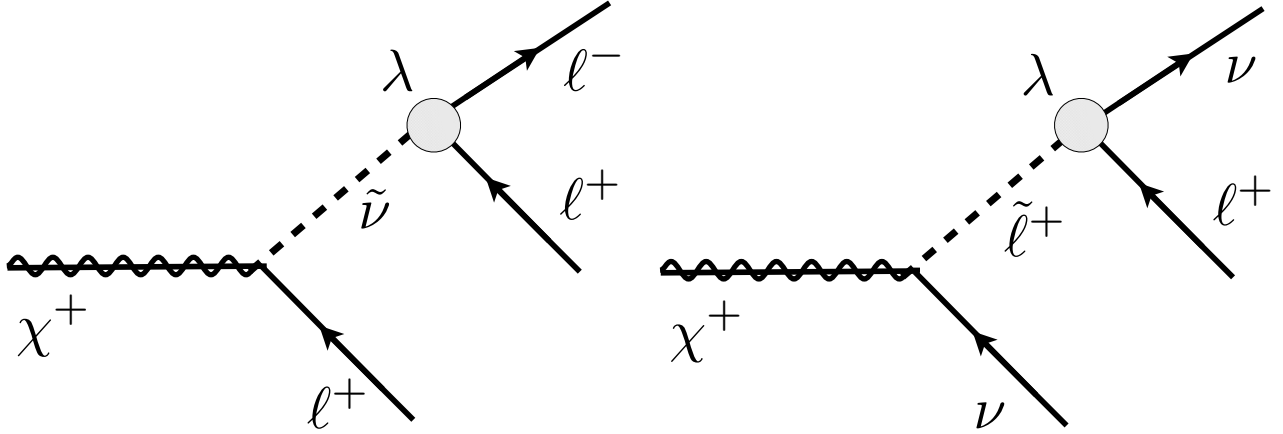


Figure 3: Feynman diagrams for decays of a chargino LSP in the  $R$ -parity violating scenario. The blob represents a tiny RPV coupling  $\lambda$ , which mediates the decay of the chargino to three charged leptons, or to one charged lepton and two neutrinos. We have suppressed lepton flavor indices, but in the text we only consider  $\lambda_{323}$  to be non-zero.

In particular it can be distinguished from (A), (B), and (C) with  $\mathcal{O}(10)$  observed events. This conclusion is insensitive to the mass of the stau, as long as it is sufficiently massive that the jets can pass the triggers and cuts.

Another observation is that considering both muons and jets in the final state topologies is necessary to distinguish the widest variety of models. For example, it might be expected that the two-body decays of a stop (C) and gluino (B) would have fairly different branching fractions to higher jet multiplicity states. However, the WIMP cascades in (B) and the secondary top quark decay in (C) lead to nearly degenerate branching fractions to different jet multiplicities for the two models. Fortunately, the two scenarios have different branching fractions to final states containing muons. With  $\mathcal{O}(100)$  observed decays, models (B) and (C) can be distinguished by their branching fraction to decays containing a single isolated muon. Likewise, the  $R$ -parity violating decay through the lepton-number violating operator (E) is easily distinguished by its large branching fraction to events containing hard muons.

Based on these analyses, we conclude that observing the branching fractions to different jet and muon multiplicities of  $\mathcal{O}(10 - 100)$  late decay events is sufficient to distinguish likely MMCP scenarios, in particular those which differ in the color representation of the meta-stable particle or the number of leptons produced in the decay. Comparing to Table 2, this corresponds for instance to direct pair production cross sections  $40 - 400$  fb and thus a mass reach of roughly  $1.0 - 1.3$  TeV for a color octet. Our methods are complementary to other proposals because they rely only on information obtained from the decay events themselves, without requiring any knowledge about the production events. In comparison, methods involving signatures in production events or

comparing total production and decay event rates suffer from uncertainties about the interactions and spectra of R-hadrons.

## 4 Determining Lorentz Structure

As we saw in Section 3, many MMCP scenarios can be distinguished by the topology of the decay. However, some scenarios could still be difficult to distinguish, for instance color octet SIMPs of different spins could have similar standard model decay modes. If an MMCP is observed to have a three-body decay, then observing the kinematic distribution of the primary decay particles provides a further test of the UV and TeV physics model by helping determine the Lorentz structure of the couplings and the MMCP and WIMP spins. In this section, we study how this information can be obtained from the kinematic properties of the final state muons and jets in an MMCP decay.

### 4.1 Decay Operators

Most of the models discussed in Section 3 yield metastable particles  $X$  because the stability of  $X$  is violated by physics at some high scale  $\Lambda$ . We can therefore integrate out the high scale physics and study the MMCP decay in each scenario through the resulting effective operator. In particular, for each effective decay operator we would like to answer the question: assuming the decay topology is compatible with a given MMCP scenario, can measurements of the late decay kinematics at the LHC provide a meaningful test of or rule out the decay operator? To answer this question, our strategy is to compare the kinematic distributions for a given scenario to a wide variety of other possible decay operators yielding similar decay topologies but different kinematic distributions.

The possible Lorentz structures and observable kinematics of the operators depend directly only on the spins, so we have listed the operators by the MMCP and WIMP spins. Table 4 lists operators involving two SM fermions ( $f = Q_L, u_R, d_R, \ell_L, e_R$ ). In listing these operators, we adopt the following notation. The letter  $X$  will of course denote the metastable particle, with  $X$  a fermion,  $\tilde{X}$  a scalar and  $\mathcal{X}$  a vector. The letter  $Y$  will be used to denote the neutral particle (WIMP) that leaves the site of the decay as missing energy, with notation otherwise identical to the metastable particle  $X$ . Three-body decays to final states involving SM bosons are also possible, but have not been included because they typically can be distinguished from our reference scenarios using the methods of Section 3 and furthermore would not significantly change our conclusions. Of course, this list is not meant to be exhaustive – the operators have however been chosen to give a wide representation of the class of dimension five and six operators which can emerge naturally from heavy physics. In particular the operator  $O_{S2}^{ff}$  corresponds to the angular distribution between the quarks in the three-body decay of the long lived gluino in Split

$J_{\text{MMCP}} \times J_{\text{WIMP}}$	Decay operators ( $ff$ modes)	
$0 \times 0$	$O_S^{ss}$	$\Lambda^{-1}(\bar{f}_R^2 f_L^1)(\tilde{X} \tilde{Y})$
	$O_V^{ss}$	$\Lambda^{-2}(\bar{f}_L^2 \gamma^\mu f_L^1)(\tilde{X} \partial_\mu \tilde{Y} - \tilde{Y} \partial_\mu \tilde{X})$
$\frac{1}{2} \times \frac{1}{2}$	$O_{S1}^{ff}$	$\Lambda^{-2}(\bar{f}_R^2 f_L^1)(\bar{Y} X)$
	$O_{S2}^{ff}$	$\Lambda^{-2}(\bar{f}_R^2 X)(\bar{Y} f_L^1)$
	$O_{V1}^{ff}$	$\Lambda^{-2}(\bar{f}_L^2 \gamma^\mu f_L^1)(\bar{Y} \gamma_\mu X)$
	$O_{T1}^{ff}$	$\Lambda^{-2}(\bar{f}_L^2 \sigma^{\mu\nu} f_R^1)(X \sigma_{\mu\nu} Y)$
	$O_{T2}^{ff}$	$\Lambda^{-2}(\bar{f}_L^2 \sigma^{\mu\nu} X)(\bar{f}_R^1 \sigma_{\mu\nu} Y)$
$1 \times 1$	$O_S^{vv}$	$\Lambda^{-1}(\bar{f}_R^2 f_L^1)(\mathcal{X}_\mu \mathcal{Y}^\mu)$
	$O_T^{vv}$	$\Lambda^{-1}(\bar{f}_R^2 \sigma^{\mu\nu} f_L^1)(\mathcal{X}_\mu \mathcal{Y}_\nu)$
	$O_{V1}^{vv}$	$\Lambda^{-2}(\bar{f}_L^2 \gamma^\mu f_L^1)(\mathcal{Y}_\nu \partial^\nu \mathcal{X}_\mu)$
	$O_{V2}^{vv}$	$\Lambda^{-2}(\bar{f}_L^2 \gamma^\mu f_L^1)(\mathcal{X}_\nu \partial^\nu \mathcal{Y}_\mu)$
	$O_{V3}^{vv}$	$\Lambda^{-2}(\bar{f}_L^2 \gamma^\mu f_L^1)(\mathcal{X}_\nu \partial_\mu \mathcal{Y}^\nu - \mathcal{Y}_\nu \partial_\mu \mathcal{X}^\nu)$
$1 \times 0$	$O_S^{vs}$	$\Lambda^{-2}(\bar{f}_R^2 f_L^1)(\mathcal{X}^\mu \partial_\mu \tilde{Y})$
	$O_V^{vs}$	$\Lambda^{-1}(\bar{f}_L^2 \gamma^\mu f_L^1)(\mathcal{X}_\mu \tilde{Y})$
	$O_T^{vs}$	$\Lambda^{-2}(\bar{f}_R^2 \sigma^{\mu\nu} f_L^1)(\mathcal{X}_\mu \partial_\nu \tilde{Y} - \mathcal{X}_\nu \partial_\mu \tilde{Y})$

Table 4: Three-body decay operators to WIMP and two SM fermions, listed by MMCP and WIMP spin. Because of the chiral nature of the SM gauge group, only chiral couplings of the SM fermions are considered. The operators for  $0 \times 1$  are the same as  $1 \times 0$  with the WIMP and MMCP interchanged and are denoted  $O_{(\quad)}^{sv}$ . For all operators the addition of the Hermitian conjugate is implied.

SUSY (see Section 3). The same operator also corresponds to the angular distribution between the tau-jets in the three-body RPV chargino decay (see Section 3) in the limit  $m_{\tilde{\ell}} \gg m_{\chi_1^+}$ .<sup>5</sup>

## 4.2 Angular Distributions

As described in Section 2.2, for each event the angles  $\theta$  between jets and muons can be measured. We wish to relate this measurements to the distribution  $dN/d\theta$  of the opening angle between the two primary SM particles in a decay, which will directly carry information about the decay

<sup>5</sup>The kinematics of the muon from the RPV chargino decay could certainly be used to improve the measurement of the tau-jet angular distribution, but for our purposes here it is sufficient to simply treat it as the invisible particle  $Y$ .

operator. The ideal situation for making this measurement would be a decay to lighter quarks ( $u, d, c, s, b$ ) or  $\mu$ , the observable signatures of which will reflect directly the primary particle kinematics up to the uncertainties due to detector resolution and parton showering as discussed in Section 2.2.1. To parametrize the detector resolution, when we estimate the efficiency of this method, we smooth the distributions by gaussian functions of width  $\Delta\theta = 10^\circ, 30^\circ$ , and  $60^\circ$ .

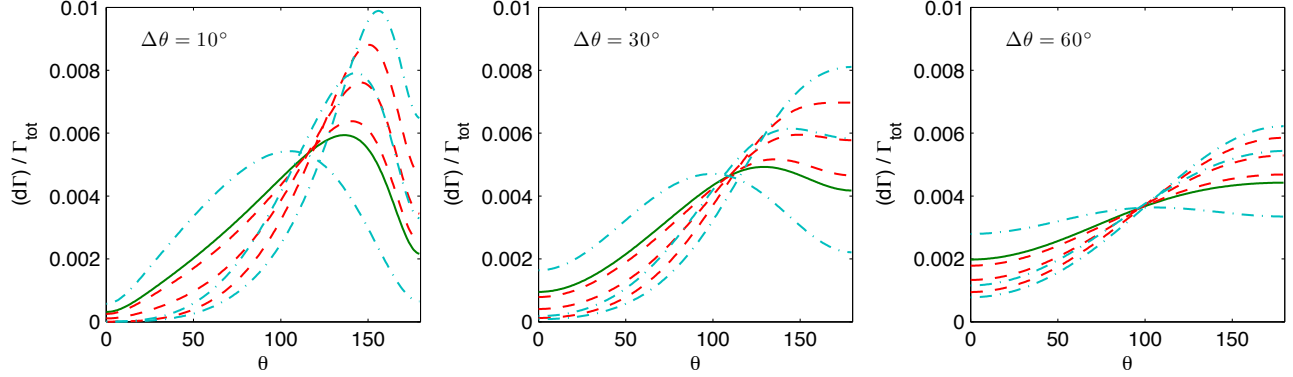


Figure 4: Selected angular distributions  $dN/d\theta$  smeared by  $\Delta\theta = 10^\circ, 30^\circ$ , and  $60^\circ$  from left to right for highly relativistic WIMP ( $m_X/m_Y = 10$ ). Solid (green): Reference Split SUSY three-body distribution  $O_{S2}^{ff}$ . Dashed (red): other representative allowed operators with same MMCP and WIMP spin and gauge representation ( $O_{T1}^{ff}, O_{T2}^{ff}, O_{S1}^{ff}$  from top to bottom on LHS). Dot-dashed (blue): operators allowed for same gauge representation but different spins ( $O_T^{vv}, O_S^{vv}, O_S^{ss}$  from top to bottom on LHS). All angular distributions shown were generated using the CompHEP and LanHEP software packages [93, 94].

The kinematic distributions for some of the representative operators in Table 4 are plotted in Figure 4. The normalized angular distributions are plotted, since the overall event rate is a priori unknown. As is evident from these plots, there are order one differences in the distributions and hence it should be possible to discriminate between operators by using simple counting statistics such as the fraction of decays occurring between two angular intervals. It is clear that we have discriminating power even with the rather coarse angular resolution assumed for the LHC detectors in Section 2. When  $\frac{M_X - M_Y}{M_Y} \gg 1$ , the distribution will be insensitive to the exact values of the WIMP and MMCP masses. Otherwise, we assume that the MMCP mass can be measured in production events and that the splitting can be determined well enough from the statistical distribution of total energy deposits to allow the appropriate distributions to be compared.

In scenarios where the event has a higher multiplicity of jets or muons due to heavy decaying primary particles ( $W, Z, h, t$ ) or cascade decays in the WIMP sector, it is more difficult to reconstruct the primary particle angular distribution. One possible strategy is to group jets to try to reconstruct the initial primary particle; for instance jets from  $W$  decay will still have an angular correlation despite the low boost factor. Another strategy, if limited jet energy resolution

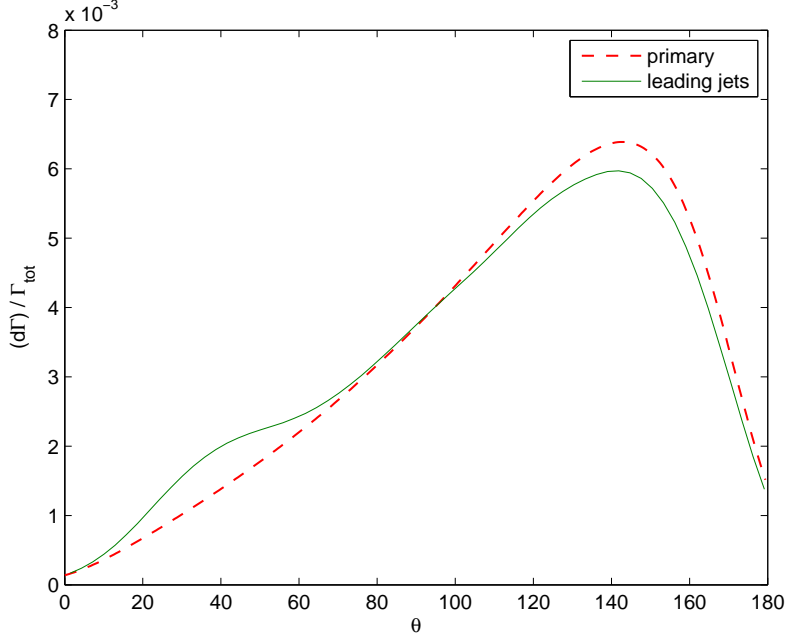


Figure 5: Angular distribution for the two leading energy jets produced in gluino decay of Model A from Table 3 including all decay modes and secondary decays (solid) compared to the angular distribution of primary quarks in the channel where only two light quarks and the WIMP are produced (dashed). The secondary decays of top quarks and chargino/neutralinos are primarily responsible for the differences in the two distributions.

is possible, would be to determine the angular distribution between the two highest energy jets in each event. Unless the secondary decays have splittings comparable to the primary decay, this distribution will tend to reflect the kinematic distribution of the primary quarks produced in the decay. To illustrate this, Figure 5 compares the normalized angular distribution between the idealized case when only primary light quarks and a WIMP are produced in the gluino decay model A (corresponding to  $O_{S2}^{ff}$ ) to the true distribution of the two leading energy jets after the heavy primary particle decays and WIMP cascade decays. As can be seen, the distribution still carries much of the original kinematic information. Therefore for the remainder of this analysis we will simply consider the distributions of the two primary SM particles produced in an event.

### 4.3 Testing MMCP Scenarios

A simple way to quantify the difference between the angular distributions of two operators is to ask how many three-body decays would need to be observed to distinguish one from another. The average number of decays necessary to distinguish two distributions can be estimated using

	$N$	$\sigma$	$M$
$\Delta\theta_{12} = 10^\circ$	23	90 fb (60 fb)	$\sim 1.2$ TeV ( $\sim 400$ GeV)
$\Delta\theta_{12} = 30^\circ$	41	160 fb (100 fb)	$\sim 1.1$ TeV ( $\sim 350$ GeV)
$\Delta\theta_{12} = 60^\circ$	130	520 fb (370 fb)	$\sim 0.9$ TeV ( $\sim 250$ GeV)

Table 5:  $N$  is the median value of the set of all  $N_i$ , the number of three-body decay events necessary to distinguish the reference operator  $O_{S2}^{ff}$  from an operator  $O_i$  in Table 4. Also shown are the approximate necessary production cross section and direct production mass reach for this number of events for a color octet SIMP (SU(2) doublet CHAMP) respectively as discussed in Section 3.

the Kullback-Leibler distance (see [95] for a description in a similar context),

$$N(O_1, O_2) = \frac{\log R}{KL(O_1, O_2)}; \quad KL(O_1, O_2) = \int d\theta \log \left( \frac{dN_1/d\theta}{dN_2/d\theta} \right) \frac{dN_1}{d\theta}, \quad (4)$$

where  $dN/d\theta$  are the normalized angular distributions, and  $R$  is the required confidence that the distribution does not correspond to the operator  $O_2$ , given that the true distribution is from  $O_1$ .

Using this statistic, in Figure 6 we estimate the number of events needed to differentiate the operators in Tables 4 from the reference Split SUSY gluino / RPV chargino distribution coming from  $O_{S2}^{ff}$ . Note that in most cases, we only need  $\sim \mathcal{O}(100)$  observed three-body decays to distinguish various operators even when the angular resolution  $\Delta\theta_{12} \approx 60^\circ$ . With better angular resolution  $\Delta\theta_{12} \approx 10^\circ$ , we can distinguish most operators with  $\sim \mathcal{O}(10)$  stopped particles. In Table 5 these numbers are converted to the necessary production cross section and corresponding mass thresholds at the 14 TeV LHC for the applicability of these tests to various UV MMCP scenarios, using the factors from Section 2.3. Assuming only direct production of MMCPs, with the most optimistic  $\Delta\theta$  resolution the 14 TeV LHC has a mass reach of 1.2 TeV (400 GeV) for testing the identity of a gluino (chargino) MMCP through the angular distribution of decays.

## 5 Conclusions

New metastable particles occur in many extensions of the Standard Model. The gravitino or axino in the MSSM, the gluino in Split SUSY, or R-parity violation give well-motivated examples of such decays. Frequently the metastable particle is charged or colored so, if light enough to be produced at the LHC, some fraction will stop in the detectors. These MMCPs then decay out of time, giving an observable and striking signature. Searches for such events are currently underway. In this work, we considered how measurements of these late decays in the LHC detectors could go beyond a detection to explore the properties of both the MMCP and the other

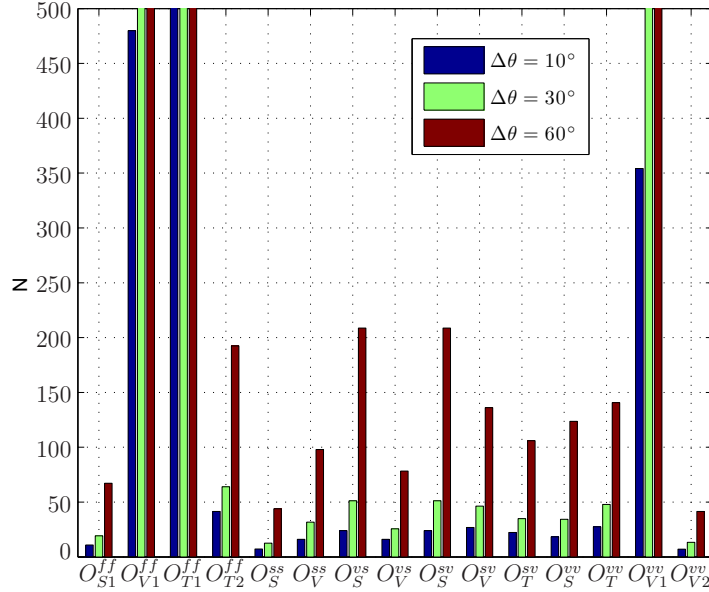


Figure 6: Average number of observed decays necessary to distinguish decay operators at 95% confidence level from the reference operator  $O_{S2}^{ff}$ , from Eq. (4) using the distributions for  $m_{X0}/m_{X8} = 10$ . For each operator, from left to right the angular resolution is  $\Delta\theta = 10^\circ, 30^\circ, 60^\circ$ .

particles, including possibly the dark matter particle, to which it decays. These decays carry much information on properties such as the spin, charge, and masses of the new particles, as well as the entire Lorentz structure of the decay operator. By determining the type of decay (two- vs three-body), identifying the particles produced, and, in the case of three-body decays, measuring the distribution of the angle between two of the produced particles, this information can be determined. This could give strong evidence for the model of the new physics, and could, for example, discriminate a decaying gluino in Split SUSY from other models.

Additionally, the decay of such a long-lived particle is often due to an accidental symmetry being broken in the UV. In this case the structure of the decay operator is determined by the UV physics giving rise to the decay. Our suggested measurements would then provide significant hints of the UV physics, far above the scales the LHC can probe directly. For example, although the squarks in Split SUSY are far above the TeV scale, they could be indirectly “observed” in this way through the out of time decays of the gluino.

We found that  $\mathcal{O}(10-100)$  observed late decays originating in the electronic barrel calorimeter of CMS or ATLAS is sufficient for discriminating many different decay operators, see Figure 6 and Table 5. Taking into account only direct production as in Table 2, this corresponds for instance to a mass reach of 1.0-1.3 TeV for a gluino at the 14 TeV LHC. With these statistics, the measured decay topologies can distinguish a variety of motivated models, in particular those differing in the color representation of the MMCP. We also found that the relative branching

fractions of decay modes differing in final state colored particle multiplicity can be measured to  $\sim 10\%$  accuracy using the example of the two and three-body decay modes of the gluino in Split SUSY. Furthermore, we showed that even in cases with degenerate decay topologies, if there is a significant branching fraction to three-body decay modes, then the kinematics of the decay can provide a nontrivial test of the MMCP and WIMP spins and the Lorentz structure of their couplings.

The measurements we have discussed can be made independently of any measurement of the MMCP properties or cross section in production events. They can therefore provide a source of information independent from other proposed measurements of the MMCP gauge and spin representation. Moreover, because the scale of physics mediating the MMCP decays is generally far above the TeV scale, late decay measurements probe physics completely inaccessible in direct production events. To fully explore this window at the LHC detectors would require a dedicated experimental effort, and we hope that this work can serve as a useful resource providing motivated theoretical benchmarks for efforts in this direction, as well as a point of reference for comparison to more exotic proposals for dedicated detectors and upgrades targeted at such metastable particles.

## Acknowledgments

We would like to thank Cliff Cheung, Sarah Eno, Tom LeCompte, Ken Rossato, Neal Weiner, David E. Kaplan, and Andy Haas for helpful discussions. DS would like to thank the Berkeley Center for Theoretical Physics for their hospitality. DS is supported in part by the NSF under grant PHY-0910467 and gratefully acknowledges support from the Maryland Center for Fundamental Physics. KH is supported by the NSF Graduate Research Fellowship under Grant No. DGE-0645962. This work was supported in part by ERC grant BSMOXFORD no. 228169.

## References

- [1] M. Drees, X. Tata, Phys. Lett. **B252**, 695-702 (1990).
- [2] A. Arvanitaki, S. Dimopoulos, A. Pierce, S. Rajendran, J. G. Wacker, Phys. Rev. **D76**, 055007 (2007). [hep-ph/0506242].
- [3] P. W. Graham, A. Ismail, S. Rajendran, P. Saraswat, Phys. Rev. **D81**, 055016 (2010). [arXiv:0910.3020 [hep-ph]].
- [4] A. Arvanitaki, S. Dimopoulos, S. Dubovsky, P. W. Graham, R. Harnik, S. Rajendran, Phys. Rev. **D79**, 105022 (2009). [arXiv:0812.2075 [hep-ph]]
- [5] J. L. Feng, A. Rajaraman, F. Takayama, Phys. Rev. **D68**, 085018 (2003). [hep-ph/0307375].



- [6] W. D. Goldberger, Y. Nomura, D. Tucker-Smith, Phys. Rev. **D67**, 075021 (2003). [hep-ph/0209158].
- [7] Y. Nomura, D. Tucker-Smith, Phys. Rev. **D68**, 075003 (2003). [hep-ph/0305214].
- [8] Y. Nomura, D. Tucker-Smith, B. Tweedie, Phys. Rev. **D71**, 075004 (2005). [hep-ph/0403170].
- [9] Y. Nomura, D. Tucker-Smith, Nucl. Phys. **B698**, 92-110 (2004). [hep-ph/0403171].
- [10] K. Cheung, G. -C. Cho, Phys. Rev. **D69**, 017702 (2004). [hep-ph/0306068].
- [11] G. Senjanovic, F. Wilczek, A. Zee, Phys. Lett. **B141**, 389 (1984).
- [12] T. Banks, M. Karliner, Nucl. Phys. **B281**, 399 (1987).
- [13] J. Bagger, S. Dimopoulos, Nucl. Phys. **B244**, 247 (1984).
- [14] N. Polonsky, S. -f. Su, Phys. Rev. **D63**, 035007 (2001). [hep-ph/0006174].
- [15] Z. Chacko, C. A. Krenke, T. Okui, JHEP **0901**, 050 (2009). [arXiv:0809.3820 [hep-ph]].
- [16] P. H. Frampton and P. Q. Hung, Phys. Rev. D **58**, 057704 (1998) [arXiv:hep-ph/9711218].
- [17] D. G. E. Walker, [arXiv:0907.3142 [hep-ph]].
- [18] D. G. E. Walker, [arXiv:0907.3146 [hep-ph]].
- [19] N. Craig, D. Stolarski, J. Thaler, [arXiv:1106.2164 [hep-ph]].
- [20] M. Fairbairn, A. C. Kraan, D. A. Milstead, T. Sjostrand, P. Z. Skands, T. Sloan, Phys. Rept. **438**, 1-63 (2007). [hep-ph/0611040].
- [21] A. R. Raklev, Mod. Phys. Lett. **A24**, 1955-1969 (2009). [arXiv:0908.0315 [hep-ph]].
- [22] S. Dimopoulos, M. Dine, S. Raby, S. D. Thomas, Phys. Rev. Lett. **76**, 3494-3497 (1996). [hep-ph/9601367].
- [23] S. Ambrosanio, G. D. Kribs, S. P. Martin, Phys. Rev. **D56**, 1761-1777 (1997). [hep-ph/9703211].
- [24] I. Hinchliffe, F. E. Paige, Phys. Rev. **D60**, 095002 (1999). [hep-ph/9812233].
- [25] R. D. Peccei, H. R. Quinn, Phys. Rev. Lett. **38**, 1440-1443 (1977).
- [26] L. Covi, H. B. Kim, J. E. Kim and L. Roszkowski, JHEP **0105**, 033 (2001) [arXiv:hep-ph/0101009].
- [27] N. Arkani-Hamed and S. Dimopoulos, JHEP **0506**, 073 (2005) [arXiv:hep-th/0405159].
- [28] For a review see: R. Barbier *et al.*, Phys. Rept. **420**, 1 (2005) [arXiv:hep-ph/0406039].
- [29] S. K. Gupta, B. Mukhopadhyaya, S. K. Rai, Phys. Rev. **D75**, 075007 (2007). [hep-ph/0701063].
- [30] S. Biswas, B. Mukhopadhyaya, Phys. Rev. **D79**, 115009 (2009). [arXiv:0902.4349 [hep-ph]].

- [31] C. Cheung, L. J. Hall and D. Pinner, arXiv:1103.3520 [hep-ph].
- [32] T. Ito, K. Nakaji, S. Shirai, [arXiv:1104.2101 [hep-ph]].
- [33] B. C. Allanach, C. M. Harris, M. A. Parker *et al.*, JHEP **0108**, 051 (2001). [hep-ph/0108097].
- [34] W. Kilian, T. Plehn, P. Richardson *et al.*, Eur. Phys. J. **C39**, 229-243 (2005). [hep-ph/0408088].
- [35] A. Heister *et al.* [ ALEPH Collaboration ], Phys. Lett. **B537**, 5-20 (2002). [hep-ex/0204036].
- [36] A. Heister *et al.* [ ALEPH Collaboration ], Eur. Phys. J. **C31**, 327-342 (2003). [hep-ex/0305071].
- [37] ALEPH, DELPHI, L3, and OPAL, *LEP2 SUSY Working Group* (2002).
- [38] V. M. Abazov *et al.* [ D0 Collaboration ], Phys. Rev. Lett. **102**, 161802 (2009). [arXiv:0809.4472 [hep-ex]].
- [39] T. Aaltonen *et al.* [ CDF Collaboration ], Phys. Rev. Lett. **103**, 021802 (2009). [arXiv:0902.1266 [hep-ex]].
- [40] V. M. Abazov *et al.* [ D0 Collaboration ], [arXiv:1110.3302 [hep-ex]].
- [41] V. Khachatryan *et al.* [ CMS Collaboration ], JHEP **1103**, 024 (2011). [arXiv:1101.1645 [hep-ex]].
- [42] G. Aad *et al.* [ ATLAS Collaboration ], Phys. Lett. **B701**, 1-19 (2011). [arXiv:1103.1984 [hep-ex]].
- [43] G. Aad *et al.* [ ATLAS Collaboration ], Phys. Lett. **B703**, 428-446 (2011). [arXiv:1106.4495 [hep-ex]].
- [44] V. Khachatryan *et al.* [ CMS Collaboration ], CMS PAS EXO-11-022 <http://cdsweb.cern.ch/record/1370057/files/EXO-11-022-pas.pdf>.
- [45] A. Rajaraman, B. T. Smith, Phys. Rev. **D76**, 115004 (2007). [arXiv:0708.3100 [hep-ph]].
- [46] R. Kitano, JHEP **0811**, 045 (2008). [arXiv:0806.1057 [hep-ph]].
- [47] T. Ito, T. Moroi, Phys. Lett. **B694**, 349-354 (2011). [arXiv:1007.3060 [hep-ph]].
- [48] M. R. Buckley, B. Echenard, D. Kahawala *et al.*, JHEP **1101**, 013 (2011). [arXiv:1008.2756 [hep-ph]].
- [49] R. Kitano, JHEP **0803**, 023 (2008). [arXiv:0801.3486 [hep-ph]].
- [50] J. L. Feng, S. T. French, I. Galon, C. G. Lester, Y. Nir, Y. Shadmi, D. Sanford, F. Yu, JHEP **1001**, 047 (2010). [arXiv:0910.1618 [hep-ph]].
- [51] R. Kitano, M. Nakamura, Phys. Rev. **D82**, 035007 (2010). [arXiv:1006.2904 [hep-ph]].

- [52] J. L. Feng, S. T. French, C. G. Lester, Y. Nir, Y. Shadmi, Phys. Rev. **D80**, 114004 (2009). [arXiv:0906.4215 [hep-ph]].
- [53] T. Ito, R. Kitano, T. Moroi, JHEP **1004**, 017 (2010). [arXiv:0910.5853 [hep-ph]].
- [54] T. Ito, Phys. Lett. **B699**, 151-157 (2011). [arXiv:1012.1318 [hep-ph]].
- [55] S. Chang, C. Kilic, T. Okui, [arXiv:1105.1332 [hep-ph]].
- [56] M. A. Luty, D. J. Phalen, [arXiv:1105.1166 [hep-ph]].
- [57] A. De Roeck, J. R. Ellis, F. Gianotti, F. Moortgat, K. A. Olive and L. Pape, Eur. Phys. J. C **49**, 1041 (2007) [arXiv:hep-ph/0508198].
- [58] K. Hamaguchi, Y. Kuno, T. Nakaya and M. M. Nojiri, Phys. Rev. D **70**, 115007 (2004) [arXiv:hep-ph/0409248].
- [59] J. L. Feng and B. T. Smith, Phys. Rev. D **71**, 015004 (2005) [Erratum-ibid. D **71**, 019904 (2005)] [arXiv:hep-ph/0409278].
- [60] K. Hamaguchi, M. M. Nojiri and A. de Roeck, JHEP **0703**, 046 (2007) [arXiv:hep-ph/0612060].
- [61] V. M. Abazov *et al.* [ D0 Collaboration ], Phys. Rev. Lett. **99**, 131801 (2007). [arXiv:0705.0306 [hep-ex]].
- [62] V. Khachatryan *et al.* [CMS Collaboration], Phys. Rev. Lett. **106**, 011801 (2011) [arXiv:1011.5861 [hep-ex]].
- [63] V. Khachatryan *et al.* [CMS Collaboration], CMS PAS EXO-11-020 <http://cdsweb.cern.ch/record/1369210/files/EXO-11-020-pas.pdf>.
- [64] W. Buchmuller, K. Hamaguchi, M. Ratz and T. Yanagida, Phys. Lett. B **588**, 90 (2004) [arXiv:hep-ph/0402179].
- [65] W. Buchmuller, K. Hamaguchi, M. Ratz and T. Yanagida, arXiv:hep-ph/0403203.
- [66] S. Asai, K. Hamaguchi, S. Shirai, Phys. Rev. Lett. **103**, 141803 (2009). [arXiv:0902.3754 [hep-ph]].
- [67] J. Pinfold and L. Sibley, Phys. Rev. D **83**, 035021 (2011) [arXiv:1006.3293 [hep-ph]].
- [68] P. Adragna, C. Alexa, K. Anderson, A. Antonaki, A. Arabidze, L. Batkova, V. Batusov, H. P. Beck *et al.*, Nucl. Instrum. Meth. **A615**, 158-181 (2010).
- [69] CMS Detector Drawings. <http://cms.web.cern.ch/cms/Resources/Website/Media/Images/Detector/DetectorDrawings/Crossnc.gif>
- [70] G. L. Bayatian *et al.* [ CMS Collaboration ].
- [71] “ATLAS: Detector and physics performance technical design report. Volume 1,” <http://atlas.web.cern.ch/Atlas/GROUPS/PHYSICS/TDR/access.html>.

- [72] B. Ille [ CMS Collaboration ], Nucl. Instrum. Meth. **A453**, 210-217 (2000).
- [73] S. Abdullin *et al.* [ CMS HCAL Collaboration ], Eur. Phys. J. **C55**, 159-171 (2008). rt,”
- [74] R. Adolphi *et al.* [ CMS Collaboration ], JINST **3**, S08004 (2008).
- [75] J. Abdallah *et al.* [ ATLAS TileCal Collaboration ], ATL-TILECAL-PUB-2008-001.
- [76] M. Martinez, [arXiv:0905.2727 [hep-ex]].
- [77] Boonekamp, M and Gianotti, F and McPherson, R A and Nessi, Marzio and Nevksi, P. ATL-GEN-2004-001, Feb 2004.
- [78] The ATLAS Collaboration, G. Aad, B. Abbott, J. Abdallah, A. A. Abdelalim, A. Abdes-selam, O. Abdinov, B. Abi, M. Abolins and H. Abramowicz Eur.Phys.J. C71 (2011) 1593. arXiv:1011.6665 [physics.ins-det]
- [79] A. C. Kraan, Eur. Phys. J. **C37**, 91-104 (2004). [hep-ex/0404001].
- [80] R. Mackeprang and A. Rizzi, Eur. Phys. J. C **50**, 353 (2007) [arXiv:hep-ph/0612161].
- [81] R. Mackeprang, D. A. Milstead, EPJ C 66 (3-4) p. 493-501.
- [82] J. L. Hewett, B. Lillie, M. Masip, T. G. Rizzo, JHEP **0409**, 070 (2004). [hep-ph/0408248].
- [83] H. Baer, B. W. Harris, M. H. Reno, Phys. Rev. **D57**, 5871-5874 (1998). [hep-ph/9712315].
- [84] G. Abbiendi *et al.* [ OPAL Collaboration ], Phys. Lett. **B572**, 8-20 (2003). [hep-ex/0305031].
- [85] M. Foster and C. Michael [UKQCD Collaboration], Phys. Rev. D **59**, 094509 (1999) [arXiv:hep-lat/9811010].
- [86] S. J. J. Gates and O. Lebedev, Phys. Lett. B **477**, 216 (2000) [arXiv:hep-ph/9912362].
- [87] J. Alwall, M. Herquet, F. Maltoni, O. Mattelaer, T. Stelzer, JHEP **1106**, 128 (2011). [arXiv:1106.0522 [hep-ph]].
- [88] A. Freitas, F. D. Steffen, N. Tajuddin, D. Wyler, JHEP **1106**, 036 (2011). [arXiv:1105.1113 [hep-ph]]
- [89] P. Meade, M. Reece, [arXiv:hep-ph/0703031].
- [90] A. Djouadi, M. M. Muhlleitner, M. Spira, Acta Phys. Polon. **B38**, 635-644 (2007). [hep-ph/0609292].
- [91] P. Gambino, G. Giudice, and P. Slavich Nucl. Phys. B, 726, 35-52 (2005).
- [92] M. Toharia, J. D. Wells JHEP 2006, 015-015 (2006).
- [93] E.Boos et al [CompHEP Collaboration], Nucl. Instrum. Meth. A534 (2004) 250 (arXiv:hep-ph/0403113); A.Pukhov et al, INP MSU report 98-41/542 (arXiv:hep-ph/9908288); CompHEP Home page: <http://comphep.sinp.msu.ru>.

- [94] A. Semenov. INP MSU Preprint 96-24/431, Moscow, 1996 (arXiv: hep-ph/9608488); A. Semenov. Nucl.Inst.&Meth. A393 (1997) p. 293; A. Semenov. INP MSU Preprint 98-2/503.
- [95] C. Cski, J. Heinonen, and M. Perelstein JHEP 2007, 107-107 (2007).